Methods for determining infrasound phase velocity direction with an array of line sensors

Kristoffer T. Walker, Mark A. Zumberge, Michael A. H. Hedlin, and Peter M. Shearer
Institute of Geophysics and Planetary Physics, Scripps Institution of Oceanography, University of California, San Diego, 9500 Gilman Drive, MC 0225, La Jolla, California 92093-0225

(Received 26 December 2007; revised 10 July 2008; accepted 10 July 2008)

Infrasound arrays typically consist of several microbarometers separated by distances that provide predictable signal time separations, forming the basis for processing techniques that estimate the phase velocity direction. The directional resolution depends on the noise level and is proportional to the number of these point sensors; additional sensors help attenuate noise and improve direction resolution. An alternative approach is to form an array of directional line sensors, each of which emulates a line of many microphones that instantaneously integrate pressure change. The instrument response is a function of the orientation of the line with respect to the signal wavefront. Real data recorded at the Piñon Flat Observatory in southern California and synthetic data show that this spectral property can be exploited with multiple line sensors to determine the phase velocity direction with a precision comparable to a larger aperture array of microbarometers. Three types of instrument-response-dependent beamforming and an array deconvolution technique are evaluated. The results imply that an array of five radial line sensors, with equal azimuthal separation and an aperture that depends on the frequency band of interest, provides directional resolution while requiring less space compared to an equally effective array of five microbarometers with rosette wind filters. © *2008 Acoustical Society of America.* [DOI: 10.1121/1.2968675]

PACS number(s): 43.60.Fg, 43.28.Dm, 43.58.Ta, 43.60.Qv [RR] Pages: 2090–2099

I. INTRODUCTION

A. Global infrasound monitoring

The acoustic frequency band beneath the human detection threshold (~18 Hz) is called infrasound. Infrasound is generated by a variety of natural and manmade sources and can travel thousands of kilometers under favorable atmospheric conditions. Nuclear explosions in the atmosphere produce far-reaching infrasound in the 0.01–10 Hz band (Landau and Lifshitz, 1959). This has recently led to increased interest in infrasound for compliance verification of the Comprehensive Nuclear Test-Ban Treaty (CTBT) [e.g., see Christie, (1999)]. The tool for this monitoring is the International Monitoring System (IMS), which is to include 60 globally distributed infrasound arrays.[1]

B. Wind noise reduction

Highly sensitive microbarometers and microphones with low-frequency response are available from a number of sources. The main difficulty in signal detection is not the sensitivity of the sensors themselves but the noise created by the wind. Increasing wind speeds correlate with increasing noise levels across the entire infrasound band. Specifically, the wind noise spectrum correlates highly with the wind velocity spectrum (Morgan and Raspet, 1992; Raspet *et al.*, 2006). One source of wind noise is the advection of spatially varying pressure or wind velocity anomalies that are frozen in time across the sensor at the local wind speed [Taylor's frozen turbulence hypothesis; see Taylor (1938)]. Because infrasound travels at much faster acoustic speeds (~330–350 m/s) than the wind and propagates across the Earth's surface at grazing elevation angles (nearly horizontal), large-aperture arrays of sensors and associated processing techniques are typically used to separate the rapidly moving signal from the more slowly moving turbulence. These techniques also provide an estimate of the azimuth toward the source and the speed with which the signal propagates across the array.

Wind noise occurs at all frequencies, and therefore the spatial separation of sensors provides only limited wind noise reduction. Spatial wind filters also help reduce wind noise. There are two types that are commonly employed: pipe networks and hose networks. Pipe networks consist of many inlet ports linked by pipes (often buried) to a central microbarometer or microphone. A common design is the "rosette" pipe filter, consisting of several clusters or rosettes of low-impedance pipe network inputs in which all inlet-microbarometer distances are the same (Alcoverro, 1998; Hedlin and Raspet, 2003; Alvocerro and Le Pichon, 2005). These rosettes vary in aperture depending on the frequency band of interest. Hedlin *et al.* (2003) and Hedlin and Alvocerro (2005) evaluated an array of rosettes. As the spatially coherent infrasound wavefront propagates across the inlets of these wind filters, the signals diffuse into the pipes and propagate toward the central sensor at the speed of sound. If wind noise originates from pressure anomalies that are advected across the array (Taylor's hypothesis) with a spatial coherence that is shorter than the separation distance between the inlets, the noise is reduced through averaging by the central sensor. This leads to a standard amplitude signal-to-noise gain of $n^{1/2}$, where n is the number of inlets. The rosette response depends on the apparent speed and frequency of the signal that propagates across the ports as well as on the rosette size. The disadvantages of rosette filters are

 0001-4966/2008/124(4)/2090/10/$23.00

that they are usually large and logistically challenging to build, the rosettes attenuate signal energy depending on the aperture (Alcoverro, 1998; Hedlin and Raspet, 2003), and resonance may occur in the infrasound band (Hedlin *et al.*, 2003). However, these filters do significantly attenuate wind noise and are employed by many of the IMS infrasound stations in arrays of up to nine elements and apertures of up to 2 km across (Hedlin and Alcoverro, 2005).

Another type of wind filter is a network of inexpensive porous hoses connected to a central microbarometer or microphone in a fashion similar to pipe arrays. Because the infrasound diffuses into the porous hose at all points of contact with the wavefront rather than a few discrete points, the signal-to-noise (SNR) ratio may be better than that for a rosette pipe array of the same aperture, depending on the spatial structure of the wind noise. These arrays are relatively simple to deploy, but their efficacy depends on their age and manufacturer (Shields *et al.*, 2007).

A more recent technique is to create a large array of many microphones and to use adaptive array processing techniques to attenuate incoherent wind noise while preserving a coherent signal (e.g., Shields, 2005). The success of this technique depends on the sensitivity of the microphones, the aperture of the array, the number and spacing of the sensors, and the processing technique employed. A disadvantage of using the standard beamforming technique with a large number of sensors is that it can require extensive computational and data-storage resources. Shields (2005) used an array of 28 sensors to investigate the optimum sensor separation distance. He showed that wind turbulence has a consistent spatial coherence for wind speeds in the 4–7 m/s range, allowing one to select the optimum sensors in the array to use in the beam for a known wind speed and direction to achieve better than $n^{1/2}$ noise reduction (where $n < 28$).

C. Motivation for this study

The optical fiber infrasound sensor (OFIS) is described by Zumberge *et al.* (2003) as a different approach to reducing wind noise. The OFIS is a compliant sealed tube that instantaneously measures pressure variation along its length by interferometrically sensing pressure-induced diameter change (Fig. 1). It spatially integrates pressure change and therefore attenuates spatially incoherent wind noise. Acoustic resonance inside the tube is not detected since standing waves are averaged to zero by the instantaneous integration along the length. These sensors can be oriented in any configuration (e.g., circle, rosette, or line). Zumberge *et al.* (2003) and Walker *et al.* (2007) showed that a single 90 m line OFIS, buried beneath 15 cm of coarse gravel, attenuates wind noise as well as a larger 70 m rosette pipe filter for winds of ~3.5 m/s. Laboratory and field measurements indicate that below 20 Hz, there is no attenuation of infrasound by the gravel (Zumberge *et al.*, 2003). For acoustic attenuation in a porous medium, the exponential decay with depth constant is proportional to the square root of the effective air flow resistance (Herrin *et al.*, 2001), suggesting that the effective flow resistance of the gravel is low.

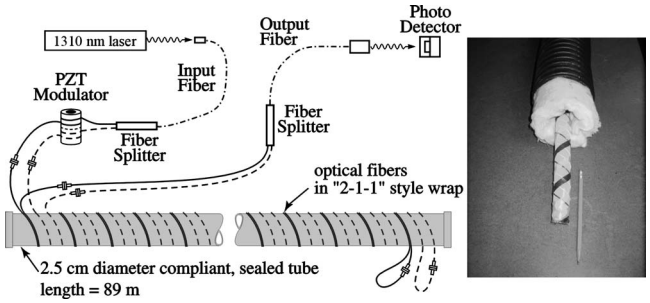

FIG. 1. Diagram and photo of an optical fiber infrasound sensor (OFIS; modified from Zumberge *et al.*, 2003). A laser illuminates two optical fibers that are helically wrapped around a sealed silicone tube. Differences in the coupling between the two optical fibers and the tube result in their responding differently to pressure-induced diameter changes, allowing an optical fiber interferometer to transform pressure changes into an optical signal. A photodetector converts the optical signal to an electrical one, which is analyzed in real time by a digital signal processor to generate a pressure recording (Zumberge *et al.*, 2004).

While the linear OFIS of length L is efficient in attenuating wind noise with less required real estate than a rosette of diameter L, its feasibility as an operational solution for infrasound data collection also depends on its ability to record infrasound reliably and to determine the direction from which the signal originated (back azimuth and elevation angle). In this paper we demonstrate three techniques for determining the phase velocity direction from an array of linear OFIS arms laid on the surface of the ground (unburied), which can generally occupy the same space as a single rosette filter. We also show how one can recover the unattenuated infrasound waveform from the OFIS recorded signals using an array deconvolution technique. The theory is presented along with applications to synthetic data and actual recordings, and conclusions are presented regarding useful OFIS array configurations.

II. SENSOR DIRECTIVITY

The velocity vector of the propagating wavefront in free space is the "phase velocity" c. The intersection of the wavefront with the Earth's surface advances at the "apparent velocity." The response of the instrument to an impulse, R, is the ratio of the recorded signal to the true pressure signal. A linear OFIS relative to a central reference point has the amplitude and phase response given by

$$R_a(f) = \mathrm{sinc}\left\{\frac{L\pi f}{c}\cos(\theta)\right\} \tag{1}$$

and

$$R_p(f) = \frac{L\pi f}{c}\cos(\theta), \tag{2}$$

where f is the frequency, L is the length of the OFIS, and θ is the angle between the phase velocity direction and the OFIS (Zumberge *et al.*, 2003, and adapted from Sheriff and Geldart (1995), p. 204). This angle is given by

$$\theta = \cos^{-1}(\cos(\theta_H)\cos(\theta_V)), \tag{3}$$

where θ_H are θ_V are the horizontal and vertical angles, respectively (Fig. 2). Equation (3) can be obtained by express-

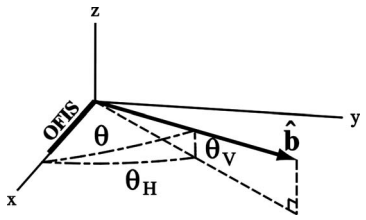

FIG. 2. Three-dimensional view of the relationship between the angles in Eq. (3). The OFIS is parallel to the x-axis, and the vector $\hat{\boldsymbol{b}}$ is antiparallel to the incident ray vector.

ing the length of the projection of $\hat{\boldsymbol{b}}$ onto the x-y plane in terms of θ_V and θ_H and by comparing this to $\hat{\boldsymbol{b}}\cdot\hat{\boldsymbol{i}}$, where $\hat{\boldsymbol{i}}$ is the unit vector in the x direction and $\hat{\boldsymbol{b}}$ is the unit vector antiparallel to the incident ray.

The phase response is just a time shift from the center of the OFIS to the end of the OFIS. For typical infrasound signals from distant sources, $\theta_V=0°-30°$ (grazing angles) and $\theta\cong\theta_H$. Figure 3(a) shows R_a as a function of θ for three typical infrasound signal frequencies. Figure 3(b) shows the variation in R_a with frequency for several sample angles. For low frequencies (or orthogonal arrival angles), the OFIS responds like a point sensor and has a flat instrument response. For all other conditions, a frequency-dependent attenuated version of the signal is recorded because the OFIS averages over some number of wave cycles. In other words, the fingerprint of the directionally dependent instrument response is recorded in the amplitude spectrum of the signal.

The OFIS impulse response can be verified numerically in the same way that the impulse response of a pipe rosette wind filter is calculated (Hedlin *et al.*, 2003). Specifically, for rays perpendicular to the OFIS, the impulse is recorded as a delta function (flat amplitude spectrum). For rays at some oblique angle to the OFIS, the impulse is averaged over time into a lower amplitude boxcar function and therefore a sinc function for the amplitude spectrum.

One might consider it a disadvantage that an OFIS spatially averages the signal. This averaging is only for wavelengths shorter than about $4L$ and only for certain directions. By comparison, a rosette filter of diameter L attenuates all signals having a wavelength shorter than about $4L$, regardless of the azimuth [Fig. 3(b); Hedlin *et al.*, 2003]. It is the

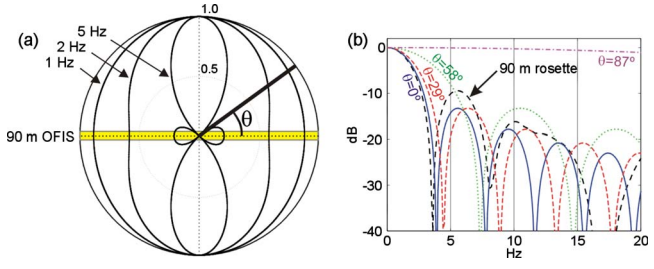

FIG. 3. (Color online) (a) Directivity and (b) frequency response R_a for a 90 m long OFIS as a function of θ and frequency [Eqs. (1) and (3)]. In (a) R_a is plotted in polar coordinates as a function of θ for three sample frequencies. In (b) R_a is plotted in dB as a function of frequency for four sample angles. For comparison purposes, the omnidirectional plane-wave response for a 90 m rosette with eight 16 m diameter secondary rosettes is also shown for grazing angles in (b).

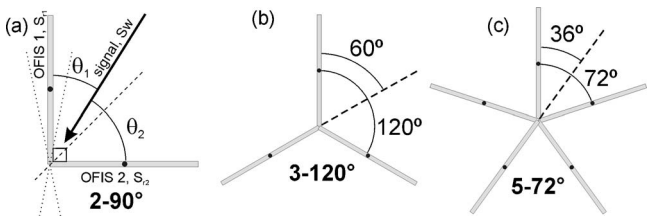

FIG. 4. OFIS array configuration naming terminology. The dotted and dashed lines in (a) are azimuths of ambiguity. The dotted azimuths can only be resolved with the separation of the OFIS centers. The dashed azimuths cannot be resolved with instrument response discrimination or separation of the OFIS centers. The angles to the dashed lines in (b) and (c) indicate the effective azimuthal separation in terms of phase-velocity-direction resolution.

directional dependence of attenuation inherent in a linear OFIS that provides additional information (besides time separation) about the direction from which a signal originated. This naturally leads to the question: Does a linear OFIS record as much directional information in the recorded amplitude spectrum as a collocated string of microphones via time separation?

In the frequency domain, each recorded OFIS signal S_r is a convolution of the signal waveform spectrum S_w with the instrument response $S_r=S_wR$. Conversely, if θ is known, one can deconvolve the instrument response to determine the signal spectrum $S_w=S_r/R$. Although the forward step is stable, the inverse step is not in this case because the denominator R has near zeros for certain frequencies (Fig. 3). To get around this problem, one can use water-level deconvolution (WLD) [e.g., see Langston 1979], which increases the amplitude of R in these troughs to, say, 2% of the maximum.

III. PHASE VELOCITY DETERMINATION TECHNIQUES

In this section, we describe the theory behind three different techniques used to derive the phase velocity direction. These techniques are a type of directional instrument-response-dependent beamforming or beam-steering. Figure 4 shows different OFIS configurations that are appropriate to use with these techniques if the length of the OFIS arms is longer than a quarter wavelength of the signal.

A. Water-level deconvolution: Predicted OFIS comparison technique

One usually wants to measure θ and the signal with the highest SNR possible. One approach is to have an array of several circular OFISs with an aperture optimized for beamforming in the frequency band of interest. However, one can exploit the directionality property of a linear OFIS by forming an array of OFIS arms in different orientations. For each possible ray orientation, an $R(\theta)$ exists that relates S_W to what should be recorded by each OFIS. Because the recorded OFIS signal is $S_r=f(S_w,\theta,L,c)$, where only S_w and θ are the unknowns, one can estimate S_w and θ if one records the signal on two OFIS with different orientations with $S_{r1}=f(S_w,\theta_1,L_1,c)$ and $S_{r2}=f(S_w,\theta_2,L_2,c)$, where θ_1 and θ_2 are related to the phase velocity direction by the array configuration [Fig. 4(a)]. One can do this by substitution, i.e., using S_{r1} to compute a predicted wave spectrum S_w^p using WLD,

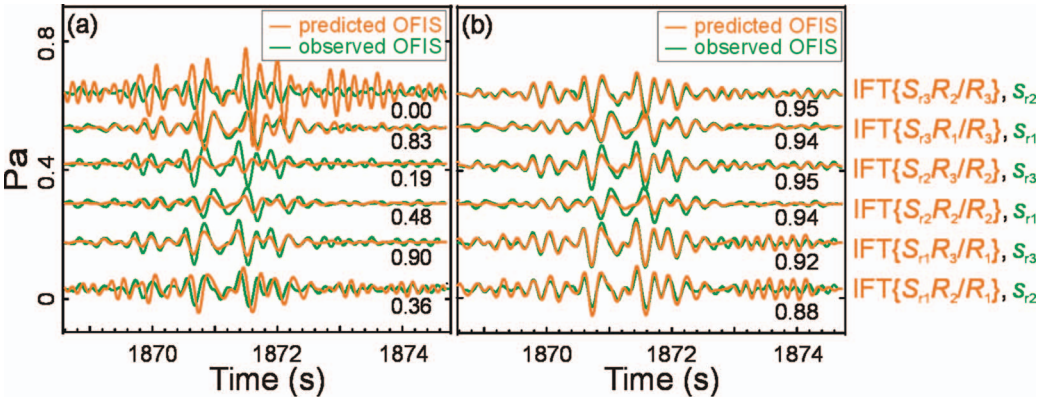

FIG. 5. Analysis of a 3°–120° OFIS signal recorded at PFO on 2005/09/20 (263) 02:31:09 UTC using the WLD technique. The predicted OFIS time series are compared with that observed for two trial back azimuths and elevation angles: (a) BAZ=316° and ELEV=44° and (b) the correct BAZ=286° and ELEV=44°. IFT is the inverse Fourier transform function. The numbers next to each pair are the correlation coefficients.

and then $S_{r2}{}^{p}=S_{w}{}^{p}R_2=S_{r1}R_2/R_1$, and performing a grid search over trial θ_t to minimize the sum of squares of the misfit between the maximum-normalized inverse Fourier transforms of S_{r2} and $S_{r2}{}^{p}$. The misfit is then given by

$$M(\theta_t)=\sum_{i=1}^{m}\left[\frac{s_{r2}{}^{p}}{\max(s_{r2}{}^{p})}-\frac{s_{r2}}{\max(s_{r2})}\right]^2, \tag{4}$$

where s_{r2} and $s_{r2}{}^{p}$ are the inverse Fourier transforms of S_{r2} and $S_{r2}{}^{p}$, respectively, and m is the number of points in the analyzed time series. The global minimum of the misfit function M corresponds to the best phase-velocity-direction estimate. We can calculate error bars by assuming that M is a measurement of a well behaved noise process [χ^2 distribution; see Jenkins and Watts (1968)] and determine the number of degrees of freedom based on the average recorded signal bandwidth (Silver and Chan, 1991), freeing us from the requirement that the observed signal samples be independent (white spectrum).

The precision using the WLD technique is mostly dependent on the SNR and the orientation of the ray with respect to the OFIS arms that are being used to estimate the waveform signal (deconvolution step). For example, in Fig. 4(a) the deconvolution of $R(\theta_1)$ from OFIS 1 (using OFIS 1 to predict OFIS 2) is more prone to noise amplification than the deconvolution of $R(\theta_2)$ from OFIS 2 (using OFIS 2 to predict OFIS 1) for the sample ray shown. There are three ways to compensate for this sensitivity. First, one can use each OFIS arm as the reference and sum both misfit functions throughout the grid search. Another approach is to skip grid points for which the trial ray is within some angle of the reference OFIS orientations (this requires more than two OFIS arms). Finally, one can use only the OFIS arm that is most perpendicular to the trial ray as the reference OFIS. Throughout this paper, we only use the first approach and sum both misfit functions for each reference OFIS. Therefore, for each grid point, $n(n-1)$ pairs of waveforms are compared, where n is the number of OFIS arms.

The 2–90° OFIS configuration has a special property [Fig. 4(a)]. The 90° separation offers identical spectral resolutions for phase velocity directions in all of the quadrants. In addition, it is computationally the fastest in part because one only needs to do the grid search within one of those quadrants to get the spectral resolution for all possible phase velocity directions. For each trial, we can therefore obtain the spectral constraints and then time shift the resulting inverse Fourier transformed waveform by $dt=(L_2\cos\theta_{H2}-L_1\cos\theta_{H1})\cos\theta_V/2c$ to calculate four separate quadrant misfit values (if we set the phase response $R_p=0$). The 2–90° configuration has been tested by analyzing recorded signals at the Piñon Flat Observatory (PFO) with the WLD method. The configuration generally only works for near-horizontally propagating signals with SNR$>$12 dB. In addition, a fundamental limitation of any two-arm OFIS configuration is that it cannot be used to determine a phase velocity direction within the vertical plane defined by the azimuth between the two OFISs [Fig. 4(a)]. Only OFIS configurations with additional elements can resolve that ambiguity.

The WLD technique can be applied to OFIS arrays having more than two elements. There is, however, a doubling of the CPU time because quadrant symmetry in a 2–90° configuration is replaced by hemisphere symmetry in larger arrays (with OFIS arms that span an azimuthal range larger than a single quadrant). For example, a real signal recorded by a 3–120° OFIS array is shown in Fig. 5. Because there are three OFIS arms, there are six pairs of traces compared for similarity at each grid point. Using a trial phase velocity direction in Fig. 5(a) that is 30° from the true direction, the predicted OFIS recordings are quite different from the observed recordings in shape and timing. A good fit (average correlation coefficient $>$0.9) is only obtained when the trial phase velocity direction is correct [Fig. 5(b)].

B. Simultaneous array deconvolution technique

The WLD technique can amplify noise because of the deconvolution step. A more stable alternative is simultaneous array deconvolution (SAD). One estimates the original signal spectrum S_w by weighting, as a function of frequency and trial phase velocity direction, the recorded spectra of the OFIS arms. For each particular frequency, some OFIS arms are positioned to provide a more accurate spectral estimate of S_w than others. For example, consider four OFIS arms (1, 2, 3, and 4) oriented at trial azimuths of 0°, 29°, 58°, and 87°,

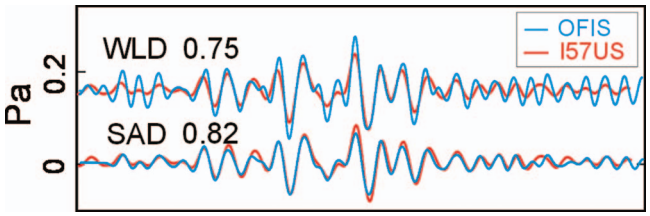

FIG. 6. Comparison of the WLD and SAD deconvolution techniques in removing the instrument responses from a 3°–120° OFIS. The resulting time series signal s_w from both techniques is compared (with correlation coefficients) to the beamformed signal from a microbarometer array.

respectively [i.e., the sample angles in Fig. 3(b)]. One should weight their estimates of the signal waveform based on the value of each response function at each frequency. In this example, the order from the highest weight to the lowest at 5 Hz would be OFIS 4, 3, 1, and 2 [comparing the responses in Fig. 3(b) at 5 Hz]. Such weighting makes the SAD technique more stable than the WLD approach because recorded spectra values around troughs in the relevant response functions are effectively eliminated from the signal estimation computation. This approach is a least-squares inversion. Assume that $\mathbf{D}$ is an $m \times n$ matrix containing the complex spectra computed from OFIS recordings, where m is the number of OFIS arms and n is the length of the spectra. The forward problem is represented in matrix notation as $\boldsymbol{GX}=\boldsymbol{D}$, where $\boldsymbol{X}=\boldsymbol{xI}$ contains S_w along the diagonal and $\boldsymbol{G}$ is an $m \times n$ matrix containing the m response functions of length n for the trial phase velocity direction. The least-squares solution for $\boldsymbol{X}$ is $\boldsymbol{X}=[\boldsymbol{G}^T\boldsymbol{G}]^{-1}\boldsymbol{G}^T\boldsymbol{D}$. Expanding for the ith frequency component, we have

$$x_i = \frac{G_{1i}D_{1i} + G_{2i}D_{2i} + \cdots + G_{mi}D_{mi}}{G_{1i}^2 + G_{2i}^2 + \cdots + G_{mi}^2}. \tag{5}$$

One can see from Eq. (5) that each x_i is a sum over the elements of $\boldsymbol{D}$ weighted by the elements of $\boldsymbol{G}$ (the response functions appropriate for that trial). This equation, which provides a least-squares estimate of S_w, is the most accurate technique when each OFIS has the same absolute noise level. From here, one can calculate the n OFIS predicted recordings in the same manner as discussed above (with the added computational load of a least-squares fit for each trial velocity direction) and derive a misfit function by comparing the n pairs of waveforms following Eq. (4). Alternatively, another measure of the misfit is the residual function in frequency space. For the trial phase velocity direction θ_t, the misfit function is given by

$$M(\theta_t) = \sum_{i=1}^{m}\sum_{j=1}^{n}(D_{ij} - G_{ij}x_j)^2. \tag{6}$$

The advantage of using the more CPU-intensive time-domain misfit of Eq. (4) is that one can normalize each waveform before taking the misfit, which allows for compensation of calibration problems and can sometimes improve stability.

A comparison of WLD and SAD for simply estimating the unattenuated signal waveforms is shown in Fig. 6. The instrument response was deconvolved from the recorded waveforms in Fig. 5. The resulting waveforms are compared with an estimate of the unattenuated signal provided by a collocated microbarometer array. WLD is performed on each OFIS recording, and their suite is averaged to give the graphed waveform. As evidenced by the correlation coefficient, the SAD waveform estimate matches the true signal more closely than does the WLD estimate, which has higher amplitudes for certain frequencies, presumably due to noise amplification.

C. Common spectrum identification technique

The common spectrum identification (CSI) technique is a search for the common signal spectrum recorded by all the OFIS arms. It does not involve deconvolution. Recall that the observed signals for two OFISs are $S_{r1}=S_wR_1$ and $S_{r2}=S_wR_2$. One can multiply both sides of these equations by the opposite instrument response function $S_{r1}R_2=S_wR_1R_2$ and $S_{r2}R_1=S_wR_2R_1$. Because of the commutative property of multiplication in the frequency domain, the right hand sides of these two equations are equal, and $S_{r1}R_2=S_{r2}R_1=Z$. We refer to Z as the common spectrum recorded by both OFIS arms. For n OFIS arms, one can perform the grid search within a hemisphere, where for each trial direction all OFIS recordings are convolved with their $n-1$ neighbor instrument responses and transformed back to the time domain (z) to evaluate the misfit function,

$$M(\theta_t) = \sum_{j=1}^{n}\sum_{i=1}^{m}\left[\frac{z_{ij}}{\max(z_j)} - \frac{\bar{z}_i}{\max(\bar{z})}\right]^2, \tag{7}$$

where $\bar{z}$ is the mean of the n estimates of z and m is the number of points in the analyzed time series. The CSI technique compares calculated waveforms that are more smoothed (because they result from convolution with multiple response functions) than any of the predicted individual OFIS recordings from the WLD or the SAD methods.

IV. RESOLUTION AND SIGNAL-TO-NOISE RATIO

Throughout this paper, SNR is referred to as excellent (SNR > 20 dB), good (SNR > 6 dB), and poor (SNR > 3.5 dB). The above OFIS array methods rely on two aspects of a recorded signal to determine its phase velocity direction: "time separation" and "instrument response discrimination." Time separation is the property that is exploited in classical array processing in either time or frequency space. Instrument response discrimination is the use of an OFIS to determine phase velocity direction based on the angular dependence of its frequency response, a characteristic of any sensor that averages along a line (Fig. 3). For example, consider a signal with a flat spectrum arriving at an OFIS with an incidence angle of 29° (one of the sample angles in Fig. 3). The spectrum of that signal recorded by that OFIS would resemble the cartoon in Fig. 7(a), where the 29° response curve from Fig. 3 leaves a fingerprint in the recorded spectrum unique to that arrival angle (or its 180° counterpart). In practice, the spectrum of the signal is unknown, which is why an array of sensors is needed to solve for both the arrival angle and the signal spectrum. Indeed,

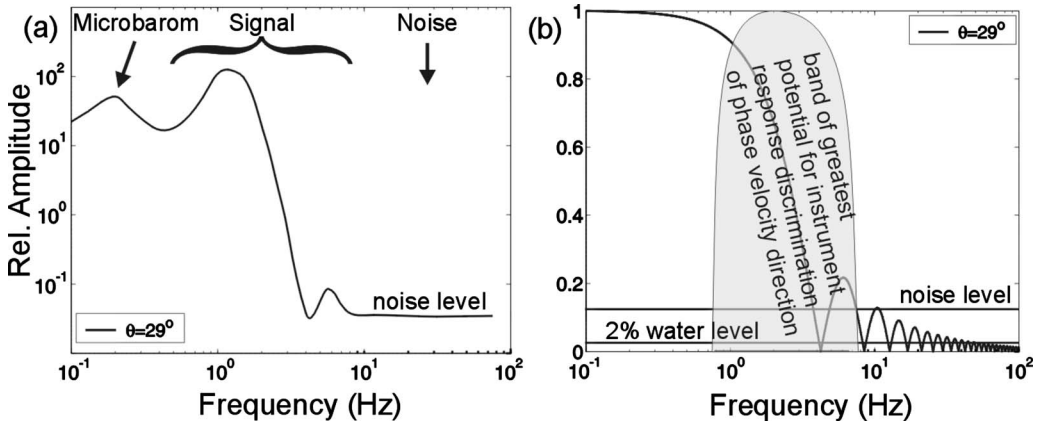

FIG. 7. Cartoon of the infrasound band that has the most leverage in determining the phase velocity direction by means of instrument response discrimination for a 90 m OFIS arm and a heuristic noise level.

the phase velocity direction of signals having spectral content mainly below $c/4L$ (around 1 Hz for a 90 m OFIS) cannot be determined with instrument response discrimination.

Noise affects the process of determining phase velocity direction in various ways for the different techniques discussed. Assuming a certain heuristic white noise level and recalling the amplitude decay of the response function at higher frequencies, one can see that certain regions of the spectrum have more leverage in determining the arrival angle for a particular SNR. As the noise floor increases, the higher signal frequencies recorded by OFIS arms at oblique angles become obscured. For this reason, it often helps to filter the recorded waveforms to isolate the band where there is the greatest potential for instrument response discrimination. Figure 7(b) depicts this region for a given SNR.

If the noise floor is above the water level used in the WLD technique, noise will be amplified, degrading the resolution by an amount dependent on the orientation and number of elements in the array. The SAD technique, on the other hand, can be more stable for higher noise floors because it assigns a weight to the *i*th frequency of all OFIS spectra based on the amplitude of the associated predicted instrument response function. This results in less contribution in the deconvolved signal from energy below noise floors that are significantly lower than the peak of the signal spectrum. However, if the absolute noise floor is much higher on one of several OFIS arms, this noise will be mapped into the deconvolved signal because SAD is a least-squares technique that can weight greatly the spectrum at certain frequencies of an uncharacteristically noisy OFIS. This noise can degrade the resolution since all OFIS comparisons are made using the noise-contaminated deconvolved signal spectrum.

The CSI method is the most stable for higher noise floors since there is no potential to amplify noise. However, because this technique heavily filters all of the OFIS recordings (including those from OFIS arms aligned parallel to the wavefront), lower frequencies (at wavelengths that are much longer than the OFIS length and separation distance) can dominate the spectrum and lead to poor phase-velocity-direction resolution. One should take care to isolate the signal energy with the appropriate high pass filter to minimize this effect.

V. APPLICATION TO REAL DATA

PFO in the southern California high desert is ensonified by many types of infrasound signals, including those originating from quarry mines, bombing ranges, sonic booms, rocket launches, and aircraft flying out of Los Angeles. During the summer of 2005, we recorded 81 infrasound signals with varying SNRs with a 3–120° OFIS array that was comprised of 90 m arms lying on the ground (unburied) at azimuths of 109.4°, 220.9°, and 330.7° (Fig. 8). The OFIS array was approximately collocated with an IMS infrasound array [I57US; see Hedlin *et al.* (2003)]. Comprised of eight elements fitted with rosette pipe filters, the IMS array data served as a reference with which to compare computed signal phase velocity directions [e.g., see Hedlin and Alcoverro (2005)]. Figure 8 shows a schematic of the high-frequency (HF) I57US subnetwork, located at the center of the I57US array with four 18 m diameter pipe rosette wind filters, each with 96 inlets spread over four 24-inlet clusters.

We analyzed all the signals recorded by the HF array and the OFIS array to empirically determine which of the OFIS methods described above yield phase velocity directions that are the most consistent with those estimated from

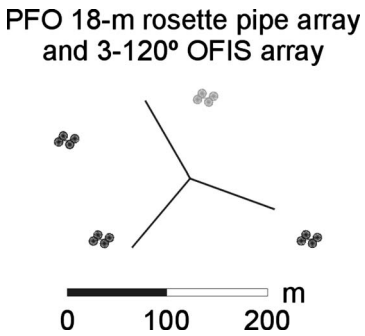

FIG. 8. PFO surface OFIS and partially buried pipe array (I57US, part of the IMS network) used in this study. The gray 18 m rosette was not used. The arrays are drawn to scale but are shown collocated for aperture comparison purposes.

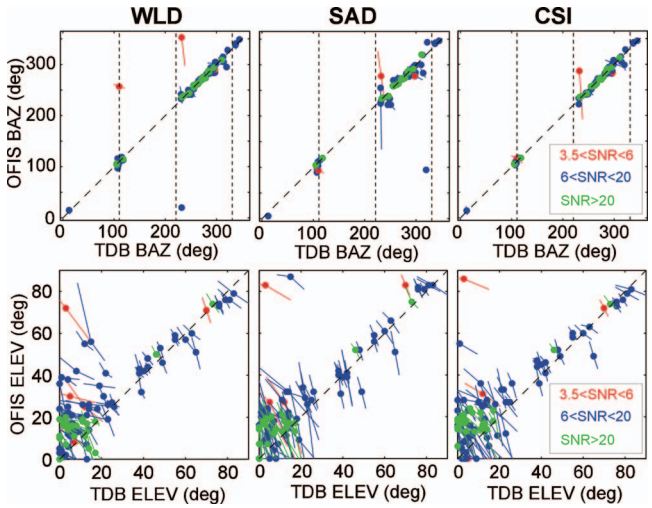

FIG. 9. Comparison of real signal back azimuths and elevation angles (recorded by a 3-120° OFIS and collocated pipe array I57US) using three OFIS methods and TDB for the pipe array. The back azimuth is the clockwise angle with respect to north. The elevation angle is the vertical angle with respect to the horizontal. SNR is the average SNR (dB) recorded by the OFIS. The 2σ error bars are the vector sums of the asymmetric error bars determined for each technique. Statistics that summarize these results are presented in Table I.

I57US array data (a known timing problem with one of the IMS data loggers limited our analysis to only three HF rosette elements). The low-frequency elements of I57US (four outer sensors with 70 m rosette filters) were also excluded from the analysis because they usually had poor SNR in the frequency band of interest.

We used a zero-phase fifth-order Butterworth bandpass filter to limit our analyses of the OFIS data to the 2–5 Hz band for the WLD and SAD techniques. The low-cut and high-cut frequencies correspond to amplitudes of −3 dB relative to the pass-band amplitude. For the CSI technique, we had the same low-cut frequency but chose a high-cut frequency of 10 Hz. This is permissible because the CSI technique does not involve deconvolution (unstable at the higher frequencies) and because it is a multifilter technique that naturally attenuates higher frequencies that are not common to all OFIS sensors. Because most of the OFIS techniques required a 2–5 Hz bandpass filter, we chose the same filter for the reference pipe array. We show results for all the signals with elevation angles of 0°–60° as determined using the pipe array. The sound speed used in the calculations was corrected for temperature.

In the following two sections, the OFIS back azimuths and elevation angles from the three techniques are compared against those obtained with time-domain beamforming (TDB) using the pipe array (Fig. 9). The TDB uncertainty is obtained using the same technique (mentioned above) as that for the OFIS methods and is therefore directly comparable. The error bars indicate the vector sum of the OFIS and TDB error bars and should intersect the unity-slope dashed line. The vertical dashed lines indicate the azimuths of the OFIS arm, where one might expect to find difficulty for some OFIS methods for low SNR. The means (μ) and standard deviations (σ) for the differences are presented in Table I. The back azimuth and elevation angle results assume that outliers are defined outside the ±25° and ±50° ranges, respectively.

TABLE I. Statistics for differences between the TDB and OFIS back azimuths and elevation angles from Fig. 9 (minus the outliers and low SNR measurements).

		Back azimuth			Elevation angle		
Method	SNR bin	μ	σ	n	μ	σ	n
WLD	All	0.4°	5.2°	79	−7.7°	11.4°	90
	SNR > 20	0.3°	2.4°	23	−6.1°	7.8°	24
	6 < SNR < 20	0.4°	6.0°	54	−8.2°	12.6°	62
SAD	All	1.7°	8.2°	77	−6.1°	8.1°	88
	SNR > 20	−0.1°	3.4°	23	−7.6°	6.1°	24
	6 < SNR < 20	1.8°	9.2°	51	−4.8°	8.6°	60
CSI	All	0.6°	4.9°	81	−6.6°	8.6°	89
	SNR > 20	0.2°	2.5°	23	−9.8°	6.7°	24
	6 < SNR < 20	0.7°	5.3°	55	−5.4°	9.0°	61

A. Back azimuth

None of the OFIS techniques shows a significant back azimuth bias. The range of standard deviations (spreads) for the WLD technique is 2°–6° depending on the SNR. Not using reference OFIS arms that are within 20° of the trial rays reduces the problems observed near the OFIS arm azimuths (because the deconvolution step is theoretically less unstable in the 2–5 Hz pass-band) but generally performs the same. Using only the most perpendicular OFIS in the deconvolution step, while theoretically better, also performs about the same. This can be explained by the reduction in the number of compared waveforms used in the misfit function (two pairs in this modified WLD versus six pairs in the unmodified WLD per trial ray).

The SAD technique has a larger spread of 3°–9°, but the outliers in WLD for azimuths close to the OFIS arms have been recovered. The SAD technique uses a more stable deconvolution method than the WLD technique. The SAD spread may be larger because one OFIS may have had an unusually high level of noise compared to the others, as discussed above.

The CSI technique has a spread of 3°–5°, comparable to the WLD spread. However, this technique eliminates all the outliers and yields measurements with associated error bars that appropriately span the unity-slope line (Fig. 9).

B. Elevation angle

There appears to be a bias of up to 10° between the OFIS estimates of elevation angle and those obtained using the pipe array. The bias, being generally less than one standard deviation, is barely significant statistically. The bias is also approximately the same for all SNRs, but it is better defined for the higher SNR signals because the error bars are smaller. It is difficult to discriminate among low elevation angles with sensors constrained to a horizontal plane; the addition of an OFIS oriented along a vertical line (on a tower, for example) may help, as would separating the OFIS arms by greater distances. It is possible that an underestima-

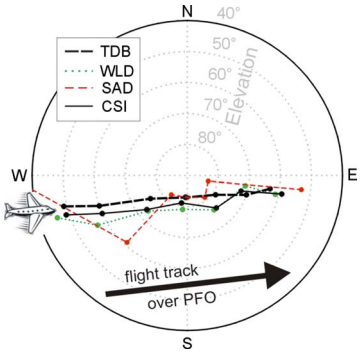

FIG. 10. (Color online) The analysis of infrasound created by an aircraft flying over PFO on 2005/09/18 (261) 19:52 UTC tracked by the OFIS array and the I57US high-frequency (HF) array 900 m to the southeast.

tion of the elevation angle by the three HF elements of the I57US array (Fig. 8) may also account for this discrepancy. Regardless, above an elevation of 30°, the differences are roughly symmetric about the unity-slope line. We performed numerical experiments that suggested that reasonable inaccuracies in the temperature-corrected sound velocity could not account for this bias. The OFIS array is located on an approximately flat surface about 900 m to the west-northwest of the I57US HF array, which is located on a slope dipping 5°–6° west. The CSI bias for easterly and westerly back azimuths is −11° and −7°, respectively. Although the slope explains the increase in the bias for easterly directions, the bias does not flip signs between the east and west as one would expect for a slope explanation.

The spread range of the elevation angles for the WLD technique is 8°–13° depending on the SNR. Above a 30° elevation, the results match better, with most of the error bars overlapping the unity-slope line. The SAD method has a spread range of 6°–9° and appears to be better at lower elevations than WLD. At higher elevations, SAD shows more scatter. The CSI technique has a comparable spread to the SAD method; the improvement seen at higher elevations mostly balances out with deterioration at lower elevations.

Many of the infrasound signals observed at PFO originate from airplanes flying overhead. These are interesting sources because the temporal variation in phase velocity direction provides a different type of comparison than that presented earlier. Figure 10 shows a polar plot of the phase velocity directions from one aircraft wavetrain broken into seven 6 s time windows. Both sensor systems tracked the plane across the sky. With respect to the other OFIS methods, the CSI method provided a track that was the most linear across the sky and the most similar to that from the pipe array. Most of the OFIS estimates are south of the estimates from the pipe array. This is likely because the arrays are not exactly collocated.

The structure of the misfit function can provide insight into the resolving power of each technique. The ideal technique results in a smooth misfit with a large dynamic range and a small confidence region. Figure 11 shows the misfit function variance (normalized sum of squares of the deviation between predicted and observed waveforms) for the three OFIS techniques compared with that provided by TDB for the signal in Figs. 5 and 6. Although the TDB estimate is well resolved, the local minima in the misfit could have been problematic had the SNR been lower. The WLD technique provides a smaller confidence region, but it too has local minima. Although the SAD method has a better dynamic range, it has prominent vertical ridges in the misfit and a vertical elongation of the confidence region, consistent with the larger elevation angle uncertainties seen in Fig. 9. The CSI misfit function is the smoothest, has the greatest dynamic range, and has the smallest confidence region.

VI. APPLICATION TO SYNTHETIC DATA

The above success in determining phase velocity direction confirms the validity of Eq. (1). Therefore, it is appropriate to create synthetic data and use the same equation to explore the power of other OFIS array configurations in determining the phase velocity direction. We created synthetic waveform data from a Vandenberg rocket launch signal recorded at I57US by an OFIS that was oriented perpendicular to the arriving infrasound wavetrain. We filtered the time series with a 2–5 Hz five-pole Butterworth bandpass filter [Fig. 12(a)]. Assuming a phase velocity direction, the filtered waveform was convolved with the appropriate response functions. White noise at a −12 dB level with respect to the original 2–5 Hz filtered signal (before convolution with the instrument response) was band limited using the same bandpass filter and was added to the result. Therefore, OFIS arms that are perpendicular to the input arrival direction have SNR = 12 dB, while OFIS arms that are at an oblique angle to the arrival direction have SNR < 12 dB.

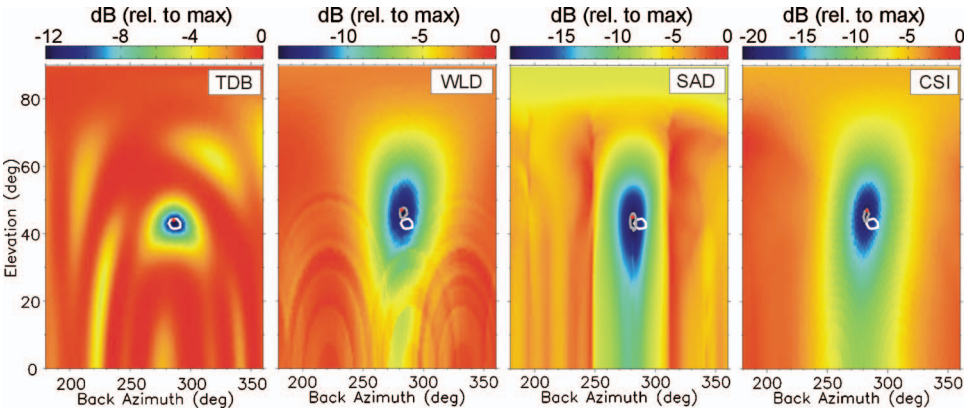

FIG. 11. Misfit functions for the three OFIS techniques and TDB (I57US HF array) used to analyze the PFO signal in Figs. 5 and 6. The 95% confidence regions of the reference TDB method (white contour) and individual OFIS methods (gray contour) are shown. The dot indicates the best estimate of the phase velocity direction (global minimum).

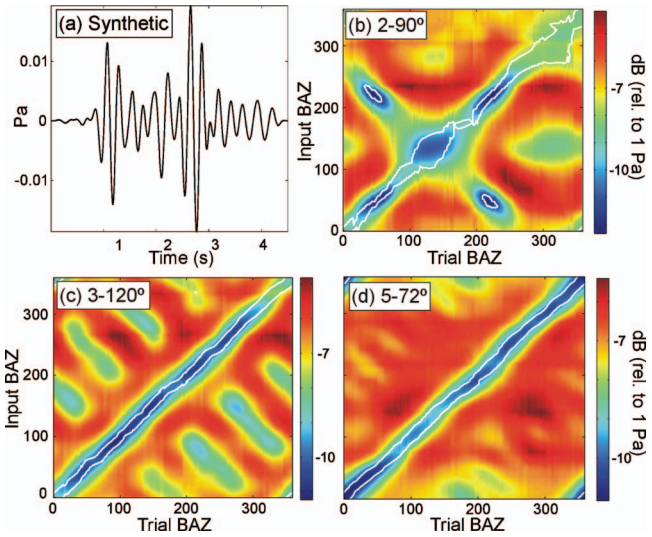

FIG. 12. Synthetic data experiments demonstrating the resolving power for phase velocity direction of different OFIS configurations using the WLD technique. The synthetic source signal is shown in (a). A misfit grid summarizing 360 different synthetic experiments (one experiment per degree input back azimuth) is shown for three different OFIS configurations in (b)–(d). White contours indicate the 95% confidence region, which ideally should enclose the unity-slope line that intersects the origin. The OFIS arms are 60 m in length.

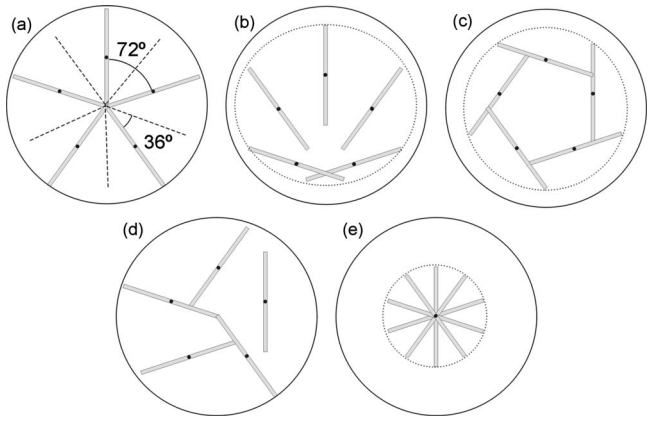

FIG. 13. Different configurations of OFIS arms of length L (drawn to scale). The circle that defines the maximum aperture of these configurations is drawn for each configuration. Configurations in (a)–(d) have the same theoretical resolving power for phase velocity direction (spectral and time separation resolution). Configuration (e) has no time separation resolution but is almost equally effective with a 75% footprint reduction. However, this configuration cannot distinguish between signals propagating from a given back azimuth and its 180° counterpart.

Comparisons up to this point have been between a 3–120° OFIS array and a three element rosette filter array. Figure 12 shows the results of analyzing horizontally propagating synthetic signals from the 0–360° back azimuth range for 2–90°, 3–120°, and 5–72° configurations. There were 360 synthetic tests (1° increment for the input back azimuth domain). For each test, the one-dimensional misfit is normalized by the 95% confidence contour. All 360 tests are plotted as a single image, the color scale of which indicates the variance of the misfit function in decibel relative to 1 Pa. For a perfect resolution, there would be a line of minima with a slope of unity intersecting the origin, reflecting that the input back azimuth for each synthetic test was recovered. In addition, the 95% confidence contours would collapse to a single line collocated with the line of minima. Finally, the variation of the misfit (or "roughness") would be insignificant compared to the depth of the minima. If the roughness were significant, then the additional off-axis local minima would tend to become possible solutions as the noise level increases.

The 2–90° configuration recovers most of the input back azimuths, but the precision varies with input back azimuth. In addition, one still observes local minima corresponding to poorly resolved ambiguities (Fig. 4). Spatial separation of the OFIS centers provides enough time separation resolution to keep these local minima above the 95% confidence contour. However, the ambiguity problem for the azimuth between the two OFIS arms is still apparent; the OFIS arms are at 0° and 90°, and the unresolved ambiguity angles are 45° and 225°.

The 3–120° configuration recovers most of the back azimuths with higher precision that does not vary with that of the input back azimuth. Although there are no unresolved ambiguities, the misfit has a high roughness.

The 5–72° configuration yields about the same precision as the 3–120° configuration. However, the misfit has a low roughness, suggesting that it would be more stable given higher noise levels. The 5–72° configuration is superior to the others because there are more OFIS arms recording the signal and because the effective azimuthal arm separation is smaller.

One can trade azimuths between OFIS arms and still preserve the original phase-velocity-direction resolving power. Although one generally wants to maximize the distance over which the coherent signal is recorded to attenuate incoherent wind noise [Fig. 13(a) radial geometry], this flexibility to trade azimuths can be attractive when logistics require the most compact footprint [36% less area than radial configuration, Fig. 13(c)] or flexibility in array installation [e.g., see Fig. 13(d)]. Since most of the resolving power of the 5–72° configuration is by means of spectral discrimination, one can collocate the OFIS centers [Fig. 13(e)] to make the smallest footprint (75% smaller than the radial configuration) as long as some method is provided to determine the hemisphere from which the signal originated.

VII. CONCLUSIONS

An array of n OFIS arms with length L inherits additional phase velocity resolution in a particular frequency band that an array of n point sensors separated by a distance L does not. One can exploit this directional fingerprint in the recorded spectra with instrument-response-dependent beamforming techniques. Each trial direction not only predicts time shifts to align the waveforms but also predicts waveform shape and amplitude changes. Real data recorded at PFO by a 3–120° OFIS array suggest that CSI outperforms other beamforming techniques that we have tested for signals with various SNRs. Of the two deconvolution techniques we tested to correct the recorded signals for the instrument response, SAD is usually better.

The PFO phase velocity directions, determined by CSI using a three-OFIS array (3–120°) with a 180 m aperture, compare favorably with those provided by three rosette elements of a roughly collocated, certified[2] IMS array with an aperture of ~250 m. This is significant because the three 90 m OFIS arms require less dedicated space than the three rosette filters.

The favorable results above are for a surface 3–120° array. An OFIS is more affected by noise on the surface than when it is buried. A single buried 90 m OFIS has a noise floor that is comparable to that provided by an entire 70 m rosette (Zumberge *et al.*, 2003; Walker *et al.*, 2007). These facts, our comparisons between different algorithms, and our synthetic tests predict that a buried 5–72° OFIS array will perform even better than a 3–120° OFIS array for infrasound measurement and characterization.

ACKNOWLEDGMENTS

We thank Petar Durdevic, Pat Walsh, Clint Coon, Eric Blum, Robin Matoza, and Joel White for their assistance with field and laboratory work. We also thank David Horwitt and David Chavez for providing data acquisition and real-time data transfer software and support. Jon Berger, Robin Matoza, and Scott DeWolf provided fruitful and inspiring discussions. We thank Mark Pickens, Bill Andre, and the U.S. Infrasound Team for their suggestions and feedback. This research was supported by the U.S. Army Space and Missile Defense Command. The High-Performance Wireless Research and Education Network (HPWREN) provided internet access to the OFIS array and microbarometer data recorded at PFO. This manuscript was improved by reviews from Richard Raspet and two anonymous reviewers.

[1]A description of the IMS is provided at http://www.seismo.ethz.ch/bsv/ctbto/ims.html (last viewed May 23, 2008).

[2]The certification of IMS arrays is discussed at http://www.ctbto.org/verification/overview.html (last viewed May 23, 2008).

Alcoverro, B. (**1998**), "Proposition d'un systeme de filtrage acoustique pour une station infrason IMS (Proposal of a filtering system for an acoustic IMS infrasound station)," Scientific Report No. 241, Commissariat a l'Energie Atomique, Departement Analyse Surveillance Environnement (Atomic Energy Commission, Department of Analysis, Surveillance, and Environment), Bruyéres-le-Châtel, France.

Alcoverro, B., and Le Pichon, A. (**2005**), "Design and optimization of a noise reduction system for infrasound measurements using elements with low acoustic impedance," J. Acoust. Soc. Am. **117**, 1717–1727.

Christie, D. (**1999**). "The infrasound segment of the CTBTO's international monitoring system," IUGG, XXII General Assmbly, B.7 (abstract).

Hedlin, M. A., Alcoverro, B., and D'Spain, G. (**2003**), "Evaluation of rosette infrasonic noise reducing spatial filters," J. Acoust. Soc. Am. **114**, 1807–1820.

Hedlin, M. A. H., and Alcoverro, B. (**2005**), "The use of impedance matching capillaries for reducing resonance in rosette infrasonic spatial filters," J. Acoust. Soc. Am. **117**, 1880–1888.

Hedlin, M. A. H., and Raspet, R. (**2003**), "Infrasonic wind noise reduction by barriers and spatial filters," J. Acoust. Soc. Am. **114**, 1379–1386.

Herrin, E., Sorrells, G. C., Negraru, P., Swanson, J. G., Golden, P., and Mulcahy, C. (**2001**), "Comparative evaluation of selected infrasound noise reduction methods," *Proceedings of the 23rd Seismic Research Review: Worldwide Monitoring of Nuclear Explosions*, 2–5 October, pp. 131–139.

Jenkins, G. M., and Watts, D. G. (**1968**), *Spectral Analysis and Its Applications* (Holden-Day, San Francisco, **1968**).

Landau, L. D., and Lifshitz, E. M. (**1959**), *Fluid Mechanics* (Pergamon, Oxford).

Langston, C. (**1979**), "Structure under Mount Rainier, Washington, inferred from teleseismic body waves," J. Geophys. Res. **84**, 4749–4762.

Morgan, S., and Raspet, R. (**1992**), "Investigation of the mechanisms of low-frequency wind noise generation outdoors," J. Acoust. Soc. Am. **92**, 1180–1183.

Raspet, R., Webster, J., and Dillion, K. (**2006**), "Framework for wind noise studies," J. Acoust. Soc. Am. **119**, 834–843.

Sheriff, R. E., and Geldart, L. P. (**1995**), *Exploration Seismology* (Cambridge University Press, Cambridge, England).

Shields, F. D. (**2005**), "Low-frequency wind noise correlation in microphone arrays," J. Acoust. Soc. Am. **117**, 3489–3496.

Shields, F. D., Dillon, K., and Howard, W. (**2007**), "Acoustical properties of porous hose wind noise filters," in Proceedings of the Acoustical Society of America, New Orleans, LA, 28 November–1 December 2007.

Silver, P. G., and Chan, W. W. (**1991**), "Shear wave splitting and subcontinental mantle deformation," J. Geophys. Res. **96**, 16429–16454.

Taylor, G. I. (**1938**), "The spectrum of turbulence," Proc. R. Soc. London, Ser. A **164**, 476–490.

Walker, K. T., Zumberge, M., Hedlin, M., Berger, J., and Shearer, P. (**2007**), "Resolving infrasound signals with arrays of optical fiber infrasound sensors (OFIS): Wind noise reduction, instrument responses, and phase velocity direction resolution," in Proceedings of the Acoustical Society of America, New Orleans, LA, 28 November–1 December 2007.

Zumberge, M. A., Berger, J., Hedlin, M., Husmann, E., Nooner, S., Hilt, R., and Widmer-Schnidrig, R. (**2003**), "An optical fiber infrasound sensor: A new lower limit on atmospheric pressure noise between 1 Hz and 10 Hz," J. Acoust. Soc. Am. **113**, 2474–2479

Zumberge, M. A., Berger, J., Dzieciuch, M. A., and Parker, R. L. (**2004**), "Resolving quadrature fringes in real time," Appl. Opt. **43**, 771–775.